ESA STUDY CONTRACT REPORT – EXECUTIVE SUMMARY

No ESA Study Contract Report will be accepted unless this sheet is inserted at the beginning of each volume of the Report.

ESA Contract No: 4000105567/12/NL/CO	SUBJECT: Atom Interferometry Test of the Weak Equivalence Principle in Space	CONTRACTOR: Astrium GmbH
* ESA CR( )No:	Executive Summary: No. of Volumes: 1 (15 pages) This is Volume No: 1	CONTRACTOR'S REFERENCE: AST

ABSTRACT: The Atom Interferometry Test of the Weak Equivalence Principle in Space (Q-WEP) is devoted to a precise measurement of the effect of gravity on matter using an atom interferometer; it tests one of the fundamental pillars of Einstein's Theory of General Relativity with high precision and thereby searches for hints of quantum effects in gravity, contributing to the exploration of one of the current frontiers in fundamental physics.

The primary science objective is the test of the universality of the free propagation of matter waves to an uncertainty in the Eötvös parameter of 1 part in 10^{14} by interferometrically tracking the propagation of matter waves in the earth's gravitational field. Secondary objectives are related to the demonstration of instrument capability for differential gravity measurements as well as differential acceleration measurements with 'long' free evolution times.

The study has been carried out within the ESA's General Studies Programme (GSP); a short outline of the activities performed is presented in this Executive Summary.

The work described in this Executive Summary was done under ESA Contract. Responsibility for the contents resides in the author or organisation that prepared it.

Authors - QWEP Study Team at: Astrium GmbH, Deutsches Zentrum für Luft- und Raumfahrt e.V. (DLR), Leibniz Universität Hannover, Institut d'Optique and CNRS - France, Office National d'Etudes et de Recherches Aerospatiales (ONERA), Humboldt-Universität zu Berlin, Observatoire de Paris SYRTE, University of Birmingham, Space Applications Services.

** NAME OF ESA STUDY MANAGER: Luigi Cacciapuoti DIV: SA DIRECTORATE: SRE	** ESA BUDGET HEADING: General Studies Program E/0600-00

* Sections to be completed by ESA

** Information to be provided by ESA Study Manager

Atom Interferometry Test of the Weak Equivalence Principle in Space

Contract No.: 4000105567/12/NL/CO

EXECUTIVE SUMMARY

QWEP Study Team

TABLE OF CONTENTS

Applicable Documents

[AD-1] Atom Interferometry Test of the Weak Equivalence Principle in Space, SoW, App. 1 to ESA ITT AO/1-6763/11/NL/AF

[AD-2] SCI-ESA-HSO-ESR-Issue1p1 'QWEP: Atom Interferometry Test of the WEP in Space'

Reference Documents

[RD-1] Atom Interferometry Test of the Weak Equivalence Principle in Space: Final Report, AI-AST-Final-Report, Issue1.0, 2013

[RD-2] Astrium GmbH Proposal No. A.2011-4177-0-1 in response to ESA ITT AO/1-6763/11/NL/AF, July 2011

[Wil04] James G. Williams, Slava G. Turyshev and Dale H. Boggs, "Lunar laser ranging tests of the equivalence principle", Class. Quantum Grav. 29 184004

[Sch08] Schlamminger S., Choi K.-Y., Wagner T. A., Gundlach J.H., Adelberger E. G., Phys. Rev. Lett., 100, 041101 (2008)

[Fra04] S. Fray, C. Alvarez Dies, T.W. Hänsch, M. Weitz, Atomic Interferometer with Amplitude Gratings of Light and Its Applications to Atom Based Tests of the Equivalence Principle, Phys. Rev. Lett. 93, 240404 (2004)

[Bon13] A. Bonnin, N. Zahzam, Y. Bidel, and A. Bresson, "Simultaneous Dual-Species Matter-Wave Accelerometer", arXiv:1307.2734v1

[Mün13] H. Müntinga, et al., ''Interferometry with Bose-Einstein Condensation in Microgravity'', Phys. Rev. Lett. 110, 093602 (2013)

[Gei11] R. Geiger, V. Ménoret, G. Stern, N. Zahzam, P. Cheinet, B. Battelier, A. Villing, F.Moron, M. Lours,Y. Bidel, A. Bresson, A. Landragin, and P. Bouyer, "Detecting inertial effects with airborne matter-wave interferometry", Nat. Comm. 2, 474 (2011)

[Lev09] T. Lévèque, A. Gauguet, F. Michaud, F. Pereira Dos Santos, and A. Landragin, "Enhancing the Area of a Raman Atom Interferometer Using a Versatile Double-Diffraction Technique", Phys. Rev. Lett. **103**, 080405 (2009).

[Zoe10] T. van Zoest, et al., ''Bose-Einstein Condensation in Microgravity'', Science **328**, 1540 (2010)

[Alt10] P. A. Altin, N. P. Robins, D. Döring, J. E. Debs, R. Poldy et al., "85Rb tunable-interaction Bose–Einstein condensate machine", Rev. Sci. Instrum. 81, 063103 (2010)

[Rud11] J. Rudolph et al., "Degenerate quantum gases in microgravity", Microgravity Sci. Technol. 23, 287-292 (2011)

List of Acronyms

ATI	Atom Interferometer
AOM	Acousto-Optic Modulator
BEC	Bose Einstein Condensate
ECDL	Extended Cavity Diode Laser
EDFA	Erbium Doped Fiber Amplifier
DFB	Distributed Feedback
IF	Interface
IGP	Ion Getter Pump
ISS	International Space Station
LS	Laser System
MOT	Magneto-Optic Trap
OB	Optical Bench
ODT	Optical Dipole Trap
PP	Physics Package
PPLN	Periodically Poled Lithium Niobate
RF	Radio Frequency
TEC	Thermoelectric Cooler
TRL	Technology Readiness Level

1 The Q-WEP study

The atom interferometry test of the Weak Equivalence Principle in space (Q-WEP) is devoted to a precise measurement of the effect of gravity on matter using an atom interferometer; it tests one of the fundamental pillars of Einstein's Theory of General Relativity with high precision and thereby searches for hints of quantum effects in gravity, contributing to the exploration of one of the current frontiers in fundamental physics.

The primary science objective [AD-2] is the test of the universality of the free propagation of matter waves to an uncertainty in the Eötvös parameter of 1 part in 10^{14} by interferometrically tracking the propagation of matter waves in the earth's gravitational field. Secondary objectives are related to the demonstration of instrument capability for differential gravity measurements as well as differential acceleration measurements with 'long' free evolution times [AD-2]. Current state-of-the-art tests based on lunar laser ranging [Wil04] and torsion balances [Sch08] found no deviation of the Eötvös ratio from zero with an uncertainty of $1 \cdot 10^{-13}$. With the successful test of the ATI this limit could be extended to matter waves with potentially higher precision. Additional benefits rely on the quantum nature of the test. The apparatus capable of executing the Eötvös test intrinsically allows to investigate the free evolution of matter waves and quantum mixtures of over several seconds.

The study has been carried out within the ESA's General Studies Programme (GSP) in accordance with [AD-1], and has been structured in four different parts whose general outlines and outcomes are shortly given hereafter.

1.1 Mission objectives and measurement strategy

The primary science objective is the test of the universality of the free propagation of matter waves to an uncertainty in the Eötvös parameter better than $1 \cdot 10^{-14}$. For a meaningful test of the WEP, the differential acceleration sensitivity has to be measured with an accuracy, which can compete with or surpass current ground based atom interferometers and other techniques like accelerometers based on macroscopic test masses; therefore the main scientific requirement is to reach a differential acceleration sensitivity of $\Delta a = 1 \cdot 10^{-14}$ g for an integration time of several months of continuous operation. More specifically [AD-2]:

SR1a: The Eötvös ratio $\eta = |\Delta a|/g = |a_{87} - a_{85}|/g$ shall be measured to an accuracy of $1 \cdot 10^{-14}$ within a total integration time of less than T_{ISS} = 4 months (10^7 s) during suitable time periods on the ISS.

Secondary objectives are related to the demonstration of instrument capability for 1) gravity gradient measurements, 2) differential acceleration measurements with long free-evolution times, and should be pursued to study the potential of the dual species atom interferometer beyond the primary objective exploiting the zero g condition without leading to further complexity in the design of the mission.

SR1b: Differential gravity shall be measured with a spectral sensitivity of at least $2 \cdot 10^{-10}$ $ms^{-2}Hz^{-1/2}$ for integration times between 18 s and 10^4 s.

The microgravity environment allows in principle to explore the regime of long free evolution of

the atomic wave-packet, with T up to several seconds. This is beneficial as the ATI acceleration sensitivity scales ~T^2. Although for the primary objective the evolution time shall be limited to ~ 1 s by the need to control systematic effects, the operation with T >> 1 s would provide an improvement of short-term sensitivity, as well as a unique demonstration of long coherence time in atom interferometry.

SR1c: Differential acceleration will be measured with a free evolution time T > 1 s up to T = 5 s and contrast larger than 50%.

The measurement strategy is represented in Figure 1; the implementation of a symmetric beam splitting [Lev09] in a Mach-Zehnder like geometry is depicted therein (Figure 1, Left); a schematic diagram of the geometry of the interferometer configuration is also provided (Figure 1, Right), including all the relevant laser beams, magnetic structures, and atom positions during loading, cooling and interferometer action. The selection of ^{87}Rb / ^{85}Rb allows for a high common-mode suppression ratio, and the low velocity spread inherent to the BECs preserves the interferometer contrast. A double diffraction scheme is suggested for the interferometer, since it is insensitive to many inertial effects due to its symmetric momentum transfer, has a superior magnetic immunity, is less sensitive to phase noise of the Raman laser, and allows for state-sensitive detection of all interferometer output ports. A single measurement cycle consists of the simultaneous generation / preparation of the two BECs, followed by the propagation in the interferometer and the detection sequence.

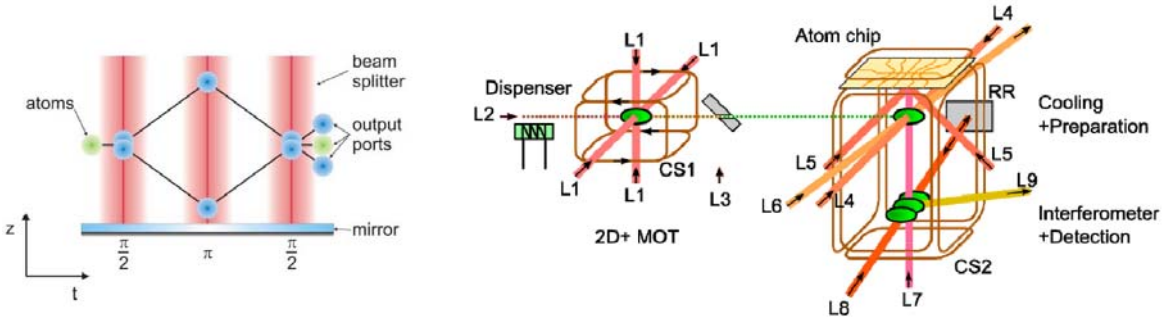

Figure 1: **Left**: Double diffraction scheme. The picture shows the implementation of a symmetric beam splitting [Lev09] in a Mach-Zehnder like interferometer geometry. It depicts a free fall situation as provided by a space born environment. **Right:** Sketch of a possible compact geometry for the Atom Interferometer (similar to the MAIUS design) including central parts like laser input ports and magnetic coils. The atom clouds at different times are shown as green circles. CS1: Ioffe-coils of 2D+MOT; CS2: 3-axis coils for generating the various fields during cooling, preparation and interferometer action; RR: Rotating retro-reflecting mirror for the Raman beam; Lx: Optical input / output port.

Since ^{85}Rb has a negative scattering length which necessitates the use of a Feshbach resonance in the condensation step, an optical dipole trap (ODT) is included in the design. To load the desired large number of atoms, a combination of a 2D+MOT and a 3D-MOT is suggested. Pre-cooling takes place in an optical molasses and by rf-evaporation in a Ioffe-Pritchard type magnetic trap. [RD-1] lists a sequence of steps for the loading and cooling procedure, including estimated durations, required laser and rf-fields and the magnetic

configuration. The total time for the procedure amounts to 8.8 s, including the initial loading, the pre-evaporation in the magnetic trap and the evaporation in the ODT. After condensation and release from the ODT, the atoms (in magnetic sensitive sub-states with mF=3 and mF=4 (for ^{87}Rb and ^{85}Rb)) will be transferred to magnetic insensitive states via a chirped rf-pulse. Subsequently, as further mitigation for the magnetic sensitivity during interferometer action, every second instrument cycle an additional state transfer to F=1 and F=2 (for ^{87}Rb and ^{85}Rb) is implemented. Furthermore, the distance between atom chip and atomic ensembles will be increased by a dedicated Raman light pulse. A possible preparation sequence is reported in [RD-1], the total time for the procedure amounts to 1 s. During interferometer action, both isotopes will be simultaneously interrogated by a $\pi/2$ - π - $\pi/2$ pulse sequence with a pulse spacing of 1 s. The sequence for the double diffraction interferometer is detailed in [RD-1]; the total time of 2-4 s is dominated by the interferometer free propagation times. Subsequently, both atom interferometer signals will be readout leading to a total cycle time of approximately 18 s (including margin). In the measurement strategy proposed, differential noise subtraction is performed by processing the output data obtained in the detection sequence.

1.2 Mission design and architecture

To achieve the science objectives, an atom interferometer has been designed including related infrastructure for accommodation on the ISS as a space platform [RD-1]. A block diagram of the general layout of the proposed instrument is sketched in Figure 2. The atom interferometer consists of three main subsystems, which are the Instrument Electronics, the Laser Assembly and the Physics Package, including the infrastructure for providing an adequate environment.

All systems are linked by optical interfaces (fibers) and electronic interfaces (rf lines, connectors). The electronics unit of the instrument provides an electronic interface to the ISS, and the entire instrument has a mechanical and thermal interface to the ISS. The electronics control the complete measurement sequence. It switches and monitors the lasers, controls the frequency detunings of the lasers via AOMs, sets the currents through the various magnetic coils and the atom chip, and reads out the CCD which detects the measurement signal.

The laser package provides all wavelengths required for atom cooling, repumping, atom transport, optical pumping, interferometer action, detection and for an optical dipole trap. Most lasers require only small output powers (< 200 mW) at a wavelength close to the Rb-D2 line at 780 nm. For some of these lasers, frequency and power stability is a crucial requirement. Only the laser for the optical dipole trap operates at a different wavelength of 1.5 µm and requires a considerable output power of 2 W total.

The third main building block of the interferometer is the physics package. To provide short loading durations, large atom numbers, and the capability to generate two-species BEC as required to achieve the main scientific objective of precise testing the WEP, a two chamber design consisting of a 2D+MOT and a 3D-MOT/interferometer chamber is proposed. This design allows for the operation with a combination of ^{87}Rb and ^{85}Rb, and is similar to the design in MAIUS / QUANTUS and STE-QUEST, exploiting synergies and avoiding redundant developments.

For all the different subsystems detailed budget estimates have been established of the required platform resources. At this level, including 20% unit margin the mass of the entire

instrument is estimated at 271 kg, the average power consumption at 740 W, and the total volume at 327 l; data rates are expected within the medium-rate link capability of the platform.

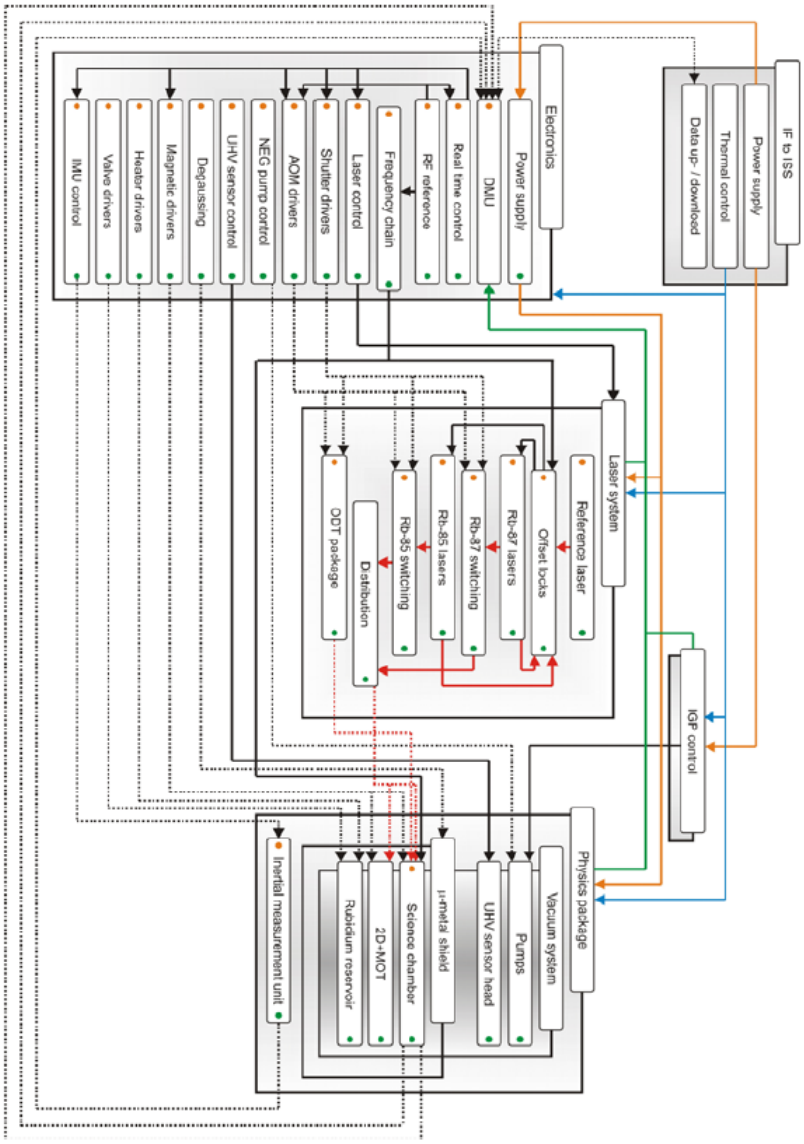

Figure 2: Instrument layout and functional architecture; red lines correspond to laser light interfaces, blue lines to thermal control, and all others to electronic interfaces; solid lines represent permanent connection, dotted a pulse mode.

To accommodate the payload, several possibilities have been considered and two of them have been identified for further assessment: an internal accommodation into the US Lab (selected as baseline at this level), and an external accommodation on the Columbus module. The two options have been comprehensively traded with respect to: a) impact on mission performance; b) restrictions imposed on the instrument (and related infrastructure) and availability of resources; c) overall complexity and cost (as driven by technical aspects); d) representativity in

terms of demonstrations for satellite-based missions. The conceptual design of the accommodation, the characterization of the space environment, and all relevant aspects related to launch / on-orbit transportation have been explored.

The key characteristics of the architecture generated during the study are summarized schematically in the following table.

Objectives	
Study	Atom Interferometry Test of the Weak Equivalence Principle in Space (QWEP)
Science Objective (Primary)	Testing the universality of the free propagation of matter waves to an uncertainty in the Eötvös parameter better than $1 \cdot 10^{-14}$.
Primary Science Requirement	SR1a: The Eötvös ratio $\eta = \lvert\Delta a\rvert/g = \lvert a_{87} - a_{85}\rvert/g$ shall be measured to an accuracy of $1 \cdot 10^{-14}$ within a total integration time of less than T_{ISS} = 4 months (10^7 s) during suitable time periods on the ISS.
Payload	
Instrument	1 Atom Interferometer with related infrastructure to guarantee adequate environment
Key subsystems	Instrument Electronics, Laser Assembly, Physics Package, and related infrastructure
Science Communications	Transfer to ground using communication channels already operating for the ISS (experiment platform)
Accomodation, orbit, mission duration	
Accomodation	ISS (internal, US Lab, see [RD-1]; trade-offs and alternatives described in [RD-1], part 2)
Baseline Orbit	ISS orbit [RD-1]
Mission duration	2 years nominal lifetime of the experiment (experiment run autonomously, remotely controlled / operated from ground)

Table 1: mission synopsis.

1.3 Instrument design aspects

The ATI operates a dual species atom interferometer measuring the differential acceleration Δa between the two isotopes ^{87}Rb and ^{85}Rb. Weighted by the acceleration g due to earth's gravitational field the Eötvös ratio η(87,85) = Δa/g is derived. Any possible violation of the equivalence principle would result in an Eötvös ratio different from zero. Due to the choice of ^{87}Rb / ^{85}Rb the interferometer has a high suppression ratio for spurious inertial perturbations and other bias terms. This is crucial in reaching the targeted single shot sensitivity and measuring the Eötvös ratio with a precision of parts in 10^{14}.

The dual ^{87}Rb / ^{85}Rb atom interferometer is based on the experience from several national activities ([Mün13], [Rud11], [Gei11]) which include DLR-funded experiments (QUANTUS / MAIUS) and CNES-funded experiments (ICE); the instrument comprises (i) a laser system to manipulate the atoms, (ii) the physics package accommodating the interferometer, and (iii) electronics for experimental control.

Laser Assembly: The laser system generating the optical frequencies for cooling, coherent manipulation and readout follows a hybrid approach. A telecom laser at 1560 nm combined with a frequency doubling will serve as frequency reference and a second high power telecom laser at 1550 nm supplies the light fields for the optical dipole trap. Laser cooling and coherent manipulation is implemented with high power diode lasers operating at 780 nm. The baseline design aims for a sub-division into different modules each fulfilling a particular function. The concept is mostly based on the functional modules developed for the sounding rocket mission MAIUS and proposed for the ATI laser system of the M-class satellite mission STE-QUEST.

The reference laser and the dipole trap laser are based on telecommunication components and frequency doubling technologies. The reference laser provides an absolute frequency reference via spectroscopy stabilization. Using frequency modulation spectroscopy (FMS) an error signal is generated and used for feedback on the laser diode for stabilization.

Microintegrated external cavitiy diode lasers (provided by the Ferdinand-Braun-Institut, Leibniz Institut für Höchstfrequenztechnik, Berlin) - combined in a Master Oscillator Power amplifier design - (µECDL-MOPAs) are suggested as laser sources for cooling, coherent manipulation and detection of ^{85}Rb and ^{87}Rb since they will combine a micro-integrated, extended cavity diode laser (µECDL) as a master oscillator laser chip (MO) and a power amplifier chip (PA) on a micro optical bench (MioB) and therefore will provide a small linewidth (< 100 kHz) and a high output power (1000 mW) at the same time. The µECDL-MOPAs are shifted to their required frequencies as specified by means of offset lock stabilization.

For switching, combining and distribution the light from the four diode laser modules is guided to one consolidated switching module and afterwards to a distribution module via pm single mode optical fibers.

Physics Package: The physics package consists of the UHV system including the 2D-MOT, the science chamber, pumps, telescopes for application of the light fields, coils and an atom chip for generating the trapping and offset magnetic fields, and a µ-metal shield to suppress external magnetic fields.

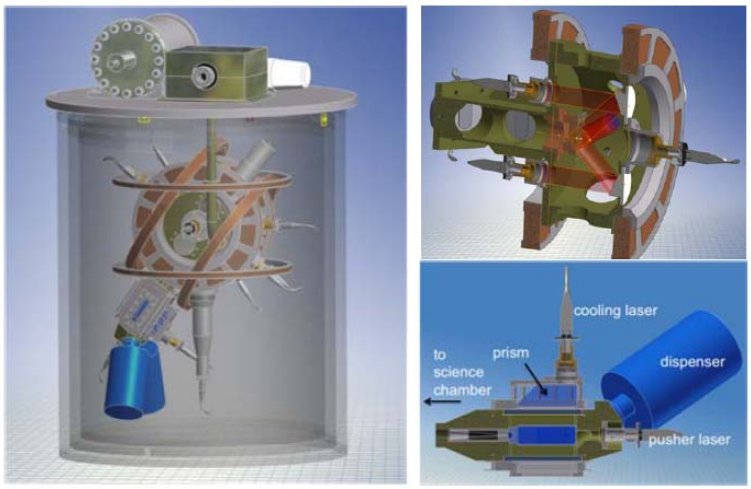

Figure 3 (Source: DLR / ZARM): **Left**: overview on instrument configuration. **Right (top)**: cross-section of the science chamber. **Right (bottom)**: 2DMOT chamber.

The dual species source for the ATI provides the necessary means for trapping and cooling the atoms until quantum degeneracy is achieved. It consists of an atom chip realizing both a MOT and a magnetic trap for pre-evaporation and an optical dipole trap where the BECs are produced. Due to the magnetic trap a high transfer efficiency from the MOT to the ODT is ensured. The latter allows to apply a magnetic field necessary to condense ^{85}Rb [Alt10].

The science chamber will feature a dodecagon design. To accommodate the interferometer with a baseline of 12 cm the inner diameter of the chamber will be 15.5 cm. The orientation of the chip defines the light field axes for the 3D-MOT and optical dipole trap (ODT). Two counter propagating beams for 3D magneto optical trapping are oriented parallel to the atom chip and superimposed with the beams for the strong axis of the ODT. The other beams for the 3D-MOT enter the chamber via the viewport above the chip and are reflected by the chip surface with an angle of 45°. To realize the crossed dipole trap a second, weak axis is needed which will enclose an angle of 22.5° with the strong axis. The ODT beam and the 3D MOT beams are superimposed by a beam splitter. The ODT beam is not retro-reflected.

Interferometry is carried out in a symmetric Mach-Zehnder like geometry with a high common mode suppression of external perturbations. During nominal operation the interferometer signal will be detected via a CCD which collects the fluorescence of the atoms. Illumination is done via the fluorescence beam which shares the interface with the Raman beam splitter. For analyzing and calibration purposes an additional absorption detection via a second CCD is foreseen. The absorption detection beam path is implemented perpendicular to the interferometer axis. All these steps are carried out under ultrahigh vacuum conditions in a chamber which is shielded against magnetic stray fields. The vacuum pump system needs to establish a vacuum at the level of 10^{-11} mbar; a combination of a passive getter pump and an ion getter pump is considered. Magnetic stray fields need to be suppressed by a factor of > 20000; a three-layer μ-metal shielding is foreseen for the physics package.

Instrument Electronics: The payload also comprises the electronics to control the experimental sequence, lasers, electromagnetic fields, RF and microwave field generation, detection, data processing and storage. The electronics consists of the following functional units: RF generation, laser control, magnet control, vacuum control, data management unit and experiment control; the latter, in particular, will control the execution of the experimental sequences (including laser pulse durations, frequencies, magnetic field durations and strengths, microwave and RF pulse durations and frequencies) for science runs as well as for calibration runs [RD-1].

1.4 Experiment performance

Statistical and systematic errors and their compatibility with the target to determine the Eötvös ratio to one part in 10^{14} are summarized hereafter. The reader is referred to [RD-1] for the corresponding detailed analysis. The number of atoms interrogated per cycle defines the fundamental limit for the sensor noise background. To meet the target sensitivity within few months of integration this is chosen to be 10^6 per species per cycle.

Vibrations and inertial motion: Vibrations and inertial motion strongly affect the output signal of a single ATI both in the form of noise above the shot-noise limit and bias above the target accuracy. The measurement strategy foresees to perform a differential between the two

simultaneous operating ^{87}Rb and ^{85}Rb interferometers. The suppression of linear vibrations in the direction of the sensitive axis relies on the simultaneous operation of the two interferometers, matched free evolution times, beam splitter pulse durations, Rabi frequencies, and effective wave vector length. Both beam splitter laser pairs for the two isotopes will be switched by the same AOM, which intrinsically matches the free evolution times and the beam splitter pulse durations.

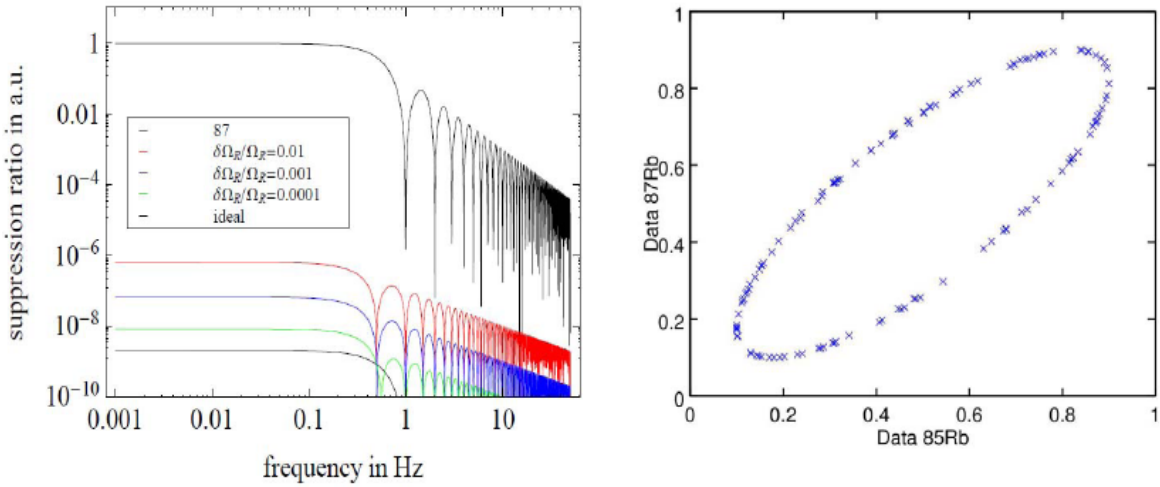

Figure 4: **Left:** suppression ratio for linear accelerations depending on the Rabi frequencies in the differential signal. The effective wave vectors are matched to $2 \cdot 10^{-9}$. **Right:** Elliptic plotting of simulated interferometer signals, i.e. raw interferometer signals for ^{85}Rb, ^{87}Rb as simulated for the vibration noise environment of the platform.

The length of the effective wave vectors will be matched on a level of 2 parts in 10^9 by choosing the detuning $\Delta\nu_{85}$ = 1.1 GHz with respect to the atomic transitions $\left|5^2 S_{1/2} F=2\right\rangle \rightarrow \left|5^2 P_{3/2} F=2\right\rangle$, $\left|5^2 S_{1/2} F=3\right\rangle \rightarrow \left|5^2 P_{3/2} F=2\right\rangle$ for ^{85}Rb and $\Delta\nu_{87}$ = 1.633 GHz with respect to the transitions $\left|5^2 S_{1/2} F=1\right\rangle \rightarrow \left|5^2 P_{3/2} F=1\right\rangle$, $\left|5^2 S_{1/2} F=2\right\rangle \rightarrow \left|5^2 P_{3/2} F=1\right\rangle$ for ^{87}Rb. The vibrational background of the platform is suppressed corresponding to Figure 4. A match of the Rabi frequencies to 1 part in 10^3 leads to an acceleration noise of $9.5 \cdot 10^{-12}$ m / s^2 which is below the shot noise limit (Table 3). The estimate of the differential acceleration bias is reported in Table 2.

Magnetic fields: Magnetic fields lead to a noise contribution and a bias if gradients are present. During interferometry the bias depends on the input state which can be alternated for subsequent interferometer cycles to relax the demand on the magnetic field homogeneity. Gradients present during the preparation of the atomic ensembles are considered more critical since those lead to a differential acceleration of the two ensembles. This impedes the matching of the starting condition and couples into the differential interferometer signal via terms of inertial motion. External stray fields will be suppressed by using multilayer μ-metal shielding. The magnetic fields outside the magnetic shield can have fluctuations as large as 8.2 G which is suppressed by the shield to 410 μG. Assuming a change of the offset field by this amount from cycle to cycle and considering key parameters and working assumptions as in Table 3, the induced noise in the differential signal is $3.9 \cdot 10^{-14}$ m / s^2.

Wavefronts: The wavefronts of the beam splitting laser affect the interferometer in three different ways. An imperfect overlap at the third beam splitting pulse reduces the interferometer contrast and thus the single shot sensitivity. A counter rotation of the retro reflection mirror will account for this. Jitter of the optics in the retro reflection path with finite surface quality induces a noise contribution indicating the need for high quality optics. Assuming a standard deviation of 100 μm of displacement of the retro reflection mirror in the two axes perpendicular to the sensitive axis of the interferometer and a surface quality of λ/300 leads to a simulated noise contribution in the differential signal of $6.8 \cdot 10^{-13}$ m / s^2 per cycle (Table 3). The finite effective wavefront curvature combined with the finite velocity spread of the atomic ensembles induces a bias. The low velocity spread of the atomic ensembles and a sufficient collimation will reduce the bias to be below the target accuracy, refer to Table 2.

Other sources: Other noise contributions arise due to the detection laser linewidth, the beam splitter laser linewidth, and the phase lock employed within the beam splitter lasers (tables below). The latter is suppressed to a negligible level due to the double diffraction. Demands on the laser linewidths are achievable with current technology. Statistical and systematic errors due to the mean field shift based on the density of the atomic clouds are estimated to be within the target accuracy and single shot sensitivity. The effect of gravity gradients onto the interferometer contrast is negligible due to the very low atomic temperature of 1 nK.

The assessment carried out at this level under the key working assumptions highlighted here (see also [RD-1]) leads to a statistical error of $4.9 \cdot 10^{-11}$ m / s^2 per cycle, dominated by the shot noise. Assuming a cycle time of 18 s a sensitivity of $6.5 \cdot 10^{-14}$ m / s^2 below the target of $g \cdot 10^{-14}$ = $8.7 \cdot 10^{-14}$ m / s^2 is reached after an integration time of 4 months. Systematic errors result in a bias of $7.98 \cdot 10^{-14}$ m / s^2, i.e. below the target of $g \cdot 10^{-14} = 8.7 \cdot 10^{-14}$ m / s^2. Basis of this estimation is a careful control of the initial differential position and velocity of the two atomic ensembles which also implies a careful control of the magnetic fields.

Error Source	Symbol	Conditions / Key Assumptions	Differential acc. bias [m/s^2]
Mean field	Δa_{mf}		$1.5 \cdot 10^{-14}$
Gravity gradient and separation	Δa_{Tz}	Δz = 4 nm	$1.0 \cdot 10^{-14}$ $5.3 \cdot 10^{-15}$
Gravity gradient and differential velocity	Δa_{Tvz}	Δv_z = 1.5 nm/s	$3.9 \cdot 10^{-15}$ $-6 \cdot 10^{-15}$
Other inertial shifts, spurious rotations	Δa_{in}	$\Omega = 10^{-6}$ rad/s, $\Delta v_x = \Delta v_y$ = 1.5 nm/s Δx = 2 μm, Δy = 0.8 μm	$1.9 \cdot 10^{-14}$
Gradient magnetic field for interferometry	Δa_{mag}	B_0 = 10 mG, δB < 27.5 μG/m	$1.0 \cdot 10^{-14}$
Raman lasers wave front	$\Delta a_{Ram,z0}$	R ~ 900 km, T_{at} = 1 nK	$3.94 \cdot 10^{-15}$
Matching of the effective wave vectors	Δa_{keff}	$\delta k/k = 2 \cdot 10^{-9}$, $a_{bias} = 10^{-7}$ m/s^2, Rabi frequency match to $1 \cdot 10^{-3}$	$6.6 \cdot 10^{-15}$

Table 2: systematic biases affecting the differential acceleration measurement.

Error Source	Symbol	Conditions / Key Assumptions	Differential acc. error per shot [m/s^2]
Shot noise	$\sigma_{\Delta a,shot}$	10^6 atoms, full contrast	$4.4 \cdot 10^{-11}$
Raman laser frequency noise	$\sigma_{\Delta a,Ram,f}$	linewidth 100 kHz, delay line 30 cm	$1.1 \cdot 10^{-11}$
Vibrational noise	$\sigma_{\Delta a,vib,long}$	k_{eff} matched to 2 parts in 10^9, Rabi frequencies matched to $1 \cdot 10^{-3}$, platform noise spectrum at night	$9.5 \cdot 10^{-12}$
Detection laser linewidth	$\sigma_{\Delta a,det,f}$		$8.5 \cdot 10^{-12}$
Gravity gradient T_{zz} and separation	$\sigma_{\Delta a,Tz}$	$\sigma_{\Delta z}$ = 2 µm (includes Coriolis)	$7.9 \cdot 10^{-12}$
Transverse mirror vibrations	$\sigma_{\Delta a,vib,trans}$	$\lambda/300$ reference object, standard deviation of displacement during beam splitting $\sigma_x = \sigma_y$ = 100 µm	$6.8 \cdot 10^{-13}$
Other inertial shifts, spurious rotations	$\sigma_{\Delta a,in}$	$\sigma_{\Delta vx} = \sigma_{\Delta vy}$ = 750 nm/s, $\sigma_{\Delta x}$ = 1 mm, $\sigma_{\Delta y}$ = 0.4 mm	$6.4 \cdot 10^{-12}$
Gravity gradient T_{zz} and differential velocity	$\sigma_{\Delta a,Tvz}$	$\sigma_{\Delta vz}$ = 750 nm/s (includes Coriolis)	$4.95 \cdot 10^{-12}$
Magnetic fields (interferometer)	$\sigma_{\Delta a,mag}$	10 % fluctuation of the offset field per cycle, 42nT/m gradient	$4.0 \cdot 10^{-14}$
Mean field	$\sigma_{\Delta a,mf}$	statistical error of 0.001 in the beam splitting ratio	$1.5 \cdot 10^{-14}$
Raman lasers wave front	$\sigma_{\Delta a,Ram,z0}$	standard deviation of 100 µm of the distance fiber coupler - lens	$2.1 \cdot 10^{-17}$
Raman laser phase lock	$\sigma_{\Delta a,Ram,p}$		$4.4 \cdot 10^{-21}$

Table 3: statistical errors in one interferometer cycle, affecting the differential measurement.

1.5 Concluding remarks

An atom interferometry test of the WEP has a strong scientific case; it addresses one of the fundamental pillars of Einstein's Theory of General Relativity and complements current efforts in fundamental physics. The instrument has been designed building on the experience from several national projects; demonstration activities have been identified to enhance the TRL. As to the platform, although an accommodation on the ISS poses stringent constraints and several challenges to the design of the experiment, nevertheless, different mitigations have been identified at this level.